



# Effect of rounded angle on the sharp corners of meta-atoms in dielectric metasurface

**YANG YANG, YASUHIKO SHIMOTSUMA,\*  MASAHIRO SHIMIZU, AND KIYOTAKA MIURA**

*Department of Material Chemistry, Graduate School of Engineering, Kyoto University, Kyoto 615-8510, Japan*

\**Shimotsuma.yasuhiko.3m@kyoto-u.ac.jp*

**Abstract:** Optical metasurfaces have attracted much attention in recent years, due to their versatile capabilities to manipulate electromagnetic waves within subwavelength scale. Dielectric metasurface holograms can significantly improve resolution, efficiency, view angle and suppression of the high order diffraction compared to traditional devices. The ability to completely control the optical properties of light using metasurface is sensitive to the geometric parameters of the nanostructures. However, current metasurface fabrication methods often result in unavoidable structural deformations. Here we introduce the rounded angles (fillets) to the sharp corners of the meta-atoms, such as rectangular pillars and isosceles triangular pillars, in dielectric metasurface and numerically study the effect of these fillets under different symmetric conditions. We find that with specific radii of the fillets, bound states in continuum (BICs) appear, making the structure act as an absorber. Apart from these BICs, fillets that do not break the original symmetry of the meta-atoms have almost no effect on the manipulation of incident light by the metasurface. However, for fillets that break the original symmetry of the meta-atoms, the amplitude and phase manipulation by metasurface may be distorted.

© 2025 Optica Publishing Group under the terms of the [Optica Open Access Publishing Agreement](#)

## 1. Introduction

Metasurfaces, ultrathin two-dimensional metamaterials with inhomogeneous sub-wavelength features, provide an exciting platform for the development of ultrathin optics. When light impinges on the nanostructures (meta-atoms) of the metasurface, abrupt phase changes, which can be controlled by the shape of the meta-atoms, are produced. Compared to conventional optical components that manipulate light by phase accumulation along the optical path, metasurfaces can modify the wavefront by introducing abrupt phase changes at the sub-wavelength scale [1]. Thanks to their remarkable capacity to manipulate electromagnetic waves within sub-wavelength scale, metasurfaces have attracted significant interest in various fields, including wavefront shaping [2,3], polarization conversion [4–6], energy concentration [7,8], holography [9–11] and so on.

One of the most attractive applications of metasurfaces is holography. Optical holography requires two steps. First, in the recording process, the phase and amplitude information of an object light is encoded as a hologram (interference fringes). Then, in the reconstructing process, the object light can be reconstructed by illuminating the hologram with reference light. With the development of spatial light modulators (SLMs) and computers, holograms can be generated by numerical calculation, called computer-generated holograms (CGHs) [12]. By using CGH, it is possible to reconstruct arbitrary objects, greatly expanding the application of holographic technology. However, CGHs generated by SLMs suffer from low resolution, low signal-to-noise ratios (SNR), and undesired high-order diffraction, due to the limitation of pixel sizes of SLMs, which are on the order of micrometers [13]. In recent years, plasmonic and high-index dielectric metasurfaces have been used to reconstruct holograms with high-quality images. Since the meta-atoms of metasurfaces can reach the sub-wavelength scale, metasurface holograms are able

to achieve higher resolution, higher efficiency, wider view angles, and suppression of high-order diffraction in the far field compared to the SLMs [14–17]. For example, a metasurface hologram made of titanium dioxide nanoparticle-embedded-resin has achieved a conversion efficiency of 96.9% [17].

To generate a metasurface hologram, the geometric parameters of the meta-atoms on the metasurface should be carefully designed. The ability to completely control the phase, amplitude, and polarization of light using metasurfaces is highly sensitive to these geometric parameters. However, in reality, it is difficult to generate meta-atoms with accurate parameters at the nanometer scale, especially the sharp corners of the meta-atoms. To make the fabrication easier, many studies have introduced rounded angles (fillets) to the corners of meta-atoms or used elliptical meta-atoms [9,18]. In this paper, we numerically demonstrated dielectric metasurfaces with triangular pillars and isosceles rectangular pillars. We then introduced fillets to the sharp corners of these pillars. In the simulations, by controlling the radius of the fillet to a specific value, we can find the bound states in continuum (BICs) and quasi-BICs, which have great potential for the super absorbers [19], sensing [20,21], optical nonlinearity enhancement [22] and so on. The effects of the fillets on the amplitude and phase shift of transmitted light are also studied systematically. We believe our studies on the fillets of the sharp corners of meta-atoms can provide guidance for generating accurate metasurface holograms, and that the BICs caused by controlling the radius of the fillets can offer a novel perspective on generating BICs.

## 2. Structure design and method

To simulate the dielectric metasurface, we use  $\text{TiO}_2$  (the refractive index is 2.61) as the material of the meta-atoms and glass (the refractive index is 1.45) as the substrate by the COMSOL MultiPhysics. The high refractive index pillars here can confine the light inside them, reducing the interferences from their neighbouring pillars. We simulate two types of meta-atoms, rectangular pillars and isosceles triangular pillars. To make sure the high efficiency, for both the rectangular pillar and the isosceles triangular pillar, the height of the pillars and the size of unit cell are fixed to 600 nm and 350 nm at the wavelength of 532 nm, respectively. By carefully designing geometric parameters of the pillars, including the width  $W$ , height  $H$  and rotation  $\theta$  as shown in Fig. 1, we can control the phase shifts after the light propagating through the pillars covering the range from 0 to  $2\pi$  with almost the same amplitude, which is necessary for the metasurface hologram. Generally, eight meta-atoms with the phase shifts in  $\pi/4$  increments are required [1].

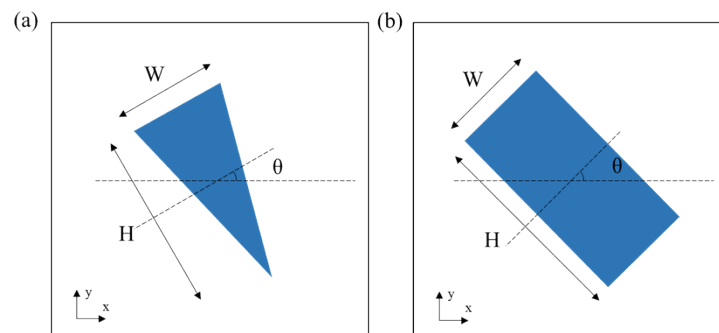


**Fig. 1.** Design of the meta-atoms. The height of the pillars is 600 nm and the size of the unit cell is 350 nm. The pillars are set at the center of the unit cell. (a) The top view of the isosceles triangular pillar determined by the height  $H$ , width  $W$  and rotation  $\theta$ . (b) The top view of the rectangular pillar determined by the height  $H$ , width  $W$  and rotation  $\theta$ .

### 3. Results and discussions

Rectangular pillars on metasurfaces have been extensively studied [6] and can be designed to function as half-wave plates. We simulate the rectangular pillars with different geometric parameters, including the height (H), width (W) and rotation angle ( $\theta$ ), and select 8 pillars as shown in Table 1 and Fig. 2(a). The  $\theta$  of these 8 pillars is fixed at  $0^\circ$ , where the transmitted light is x-polarized while the incident light is also x-polarized. As mentioned before, these rectangular pillars can function as half-wave plates, allowing us to obtain y-polarized transmitted light by changing  $\theta$  to  $45^\circ$ , as shown in Fig. 2(b). Here the amplitude of the incident light is about 27446 V/m.

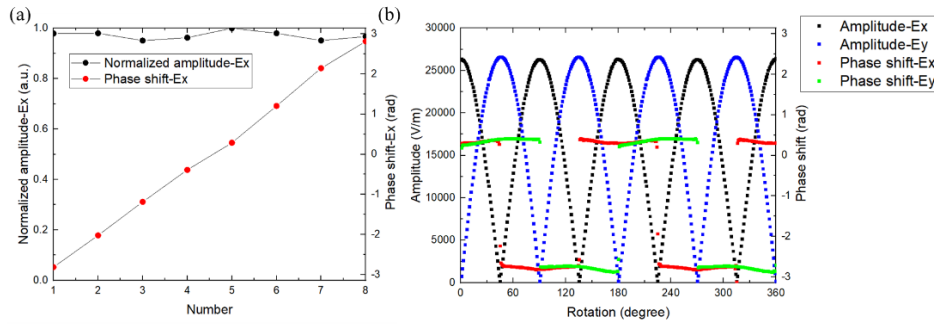


**Fig. 2.** (a) The amplitudes and the phase shifts of the x-polarized transmitted light after propagating through the eight chosen rectangular pillars for the x-polarized incident light. (b) The half-wave plate behavior of the rectangular pillar 1 in Table 1.

**Table 1. The geometric parameters of the designed rectangular pillars**

Pillar number	1	2	3	4	5	6	7	8
Height/nm	246	214	194	186	112	108	100	86
Width/nm	112	108	100	86	246	214	194	186
Phase shift/rad	-2.81	-2.02	-1.18	-0.38	0.28	1.20	2.14	2.81

On the other hand, isosceles triangular pillars have been rarely studied. Here we use the same method as for the rectangular pillars to simulate the isosceles triangular pillars on metasurfaces. The geometric parameters we control for the isosceles triangular pillars are height (H), width (W) and rotation angle ( $\theta$ ). We also select 8 pillars, as shown in Table 2 and Fig. 3(a), covering  $2\pi$  while the transmitted light and incident light are both x-polarized. Unlike rectangular pillars, isosceles triangular pillars cannot be designed as half-wave plates. Figure 3(b) shows the amplitude and phase shift of the transmitted light while rotating the isosceles triangular pillar 1 in Table 2. Although the isosceles triangular pillars do not have center symmetry, the modulations to the transmitted lights are almost the same for the rotations of  $\theta$  and  $\theta+180^\circ$ . Additionally, for the rotations of  $\theta$  ( $<180^\circ$ ) and  $180^\circ-\theta$ , the modulations to the x-polarized transmitted lights are also the same, while the modulations to the y-polarized transmitted light have a phase shift of  $\pi$ . Therefore, the modulation of the isosceles triangular pillars to the transmitted light is strongly dependent on the rotation of the axis of mirror symmetry.

After identifying the 8 pillars whose phase shifts cover the entire  $2\pi$  range, we introduce fillets to the sharp corners of these pillars, as shown in Fig. 4. For the rectangular pillars, we introduce fillets to 1 corner, 2 diagonal corners, 2 mirror symmetric corners, 3 corners, and 4 corners. As for the isosceles triangular pillars, we introduce fillets to 1 corner, 2 symmetric corners, 2 asymmetric corners, and 3 corners. The symmetric condition of each case is different, resulting

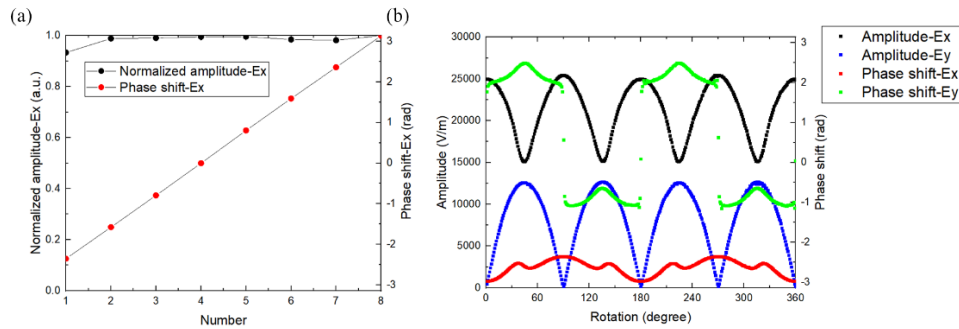


**Fig. 3.** (a) The amplitudes and the phase shifts of the x-polarized transmitted light after propagating through the eight chosen isosceles triangular pillars for the x-polarized incident light. (b) The amplitude and the phase shift of the transmitted light for the isosceles triangular pillar 1 in Table 2, as a function of  $\theta$ .

**Table 2. The geometric parameters of the designed isosceles triangular pillars**

Pillar number	1	2	3	4	5	6	7	8
Width/nm	200	300	200	120	280	280	260	300
Height/nm	180	130	100	190	210	170	150	150
Rotation/deg	90	90	0	0	0	0	0	90
Phase shift/rad	-2.35	-1.57	-0.79	0	0.80	1.59	2.36	-3.13

in varying effects on the amplitude and phase shift of transmitted light. The radius of the fillets is varied from 1 nm to the maximum.

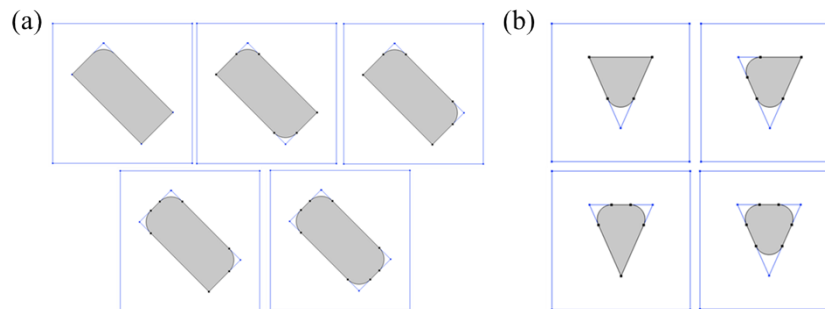


**Fig. 4.** The fillets we introduce to (a) rectangular pillars and (b) isosceles triangular pillars.

These fillets can be briefly categorized based on whether they break the mirror symmetry of the original shape or not. For rectangular pillars, 1 fillet, 2 diagonal fillets and 3 fillets break the original symmetry, while 2 symmetric fillets and 4 fillets don't break the original symmetry. The amplitudes and phase shifts (shown in the inset) of the transmitted lights with 2 symmetric fillets of rectangular pillars, where the symmetry is maintained, are shown in Fig. 5. The case of 4 fillets is shown in Fig. S1 (Supplement 1). As the radius of the fillets increases, the amplitudes of the transmitted light remain almost unchanged, while the phase shifts of the transmitted light gradually increase. However, at certain specific fillet radii, the amplitude of the transmitted light drops to 0 and the phase shift experiences an abrupt change. This is due to the BIC controlled by parameter tuning [23]. The phase shift may be related to the relative locations of complex-valued singularities, including poles and zeros [24].

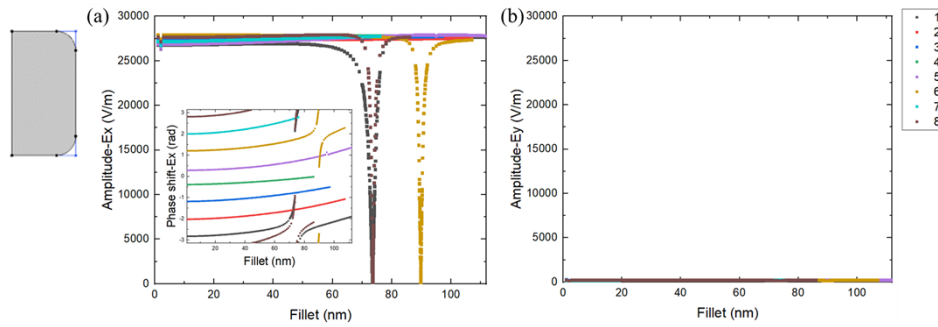


**Fig. 5.** The effect of the 2 symmetric fillets of rectangular pillars on the amplitudes and the phase shifts of the transmitted light for (a) x-polarization and (b) y-polarization.

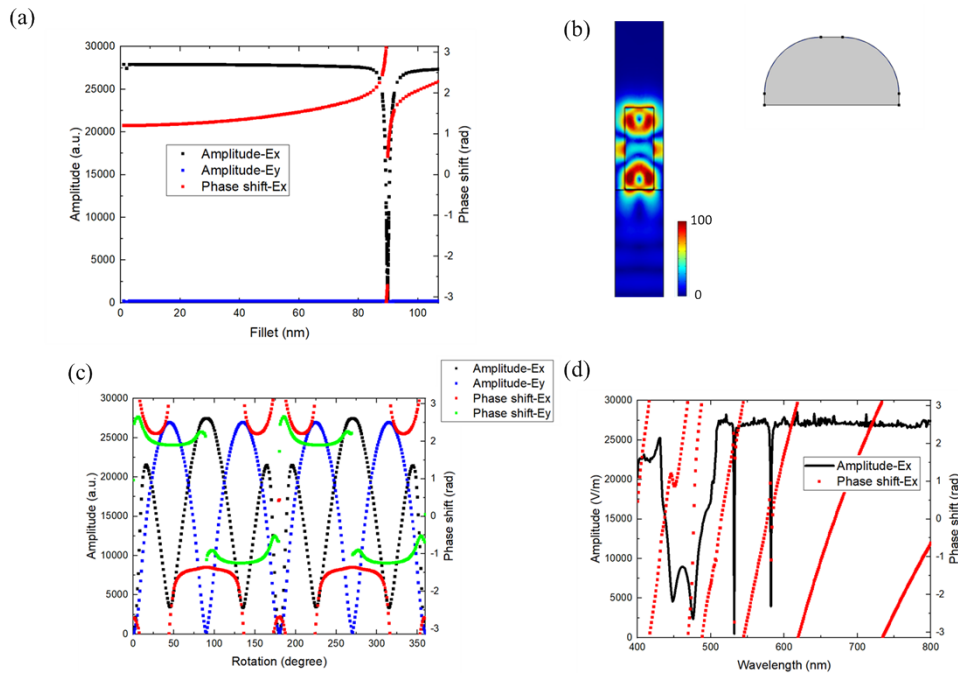


**Fig. 6.** (a) The amplitude and the phase shift variation with the fillet in the case of 2 symmetric fillets of rectangular pillar 6. (b) The energy density, (c) the amplitude and phase shift of the transmitted light and (d) the wavelength-dependent spectrum when x-polarized light is transmitted through the rectangular pillar 6 from the bottom to the top with 2 symmetric fillets at the fillet radius of 89.76 nm. The top view of the model is shown at the top right of the figure.

Typical results owing to BIC are shown in Fig. 6(a) when 2 symmetric fillets are introduced to rectangular pillar 6. The transmittance when the fillet radius is 89.76 nm is almost 0, meaning that the energy of light is completely confined within the pillar, as shown in Fig. 6(b). Around the specific fillet radii of BIC, quasi-BICs exist, where the energy is not completely confined within the pillar but leaks to the far field. The phase shift of the transmitted light around the BIC experiences an abrupt change; however, the overall trend of the phase shift remains consistent if the BIC and quasi-BIC are ignored. The half-wave plate behavior of the rectangular pillar also disappears around the BICs, as shown in Fig. 6(c). The wavelength-dependent spectrum is also

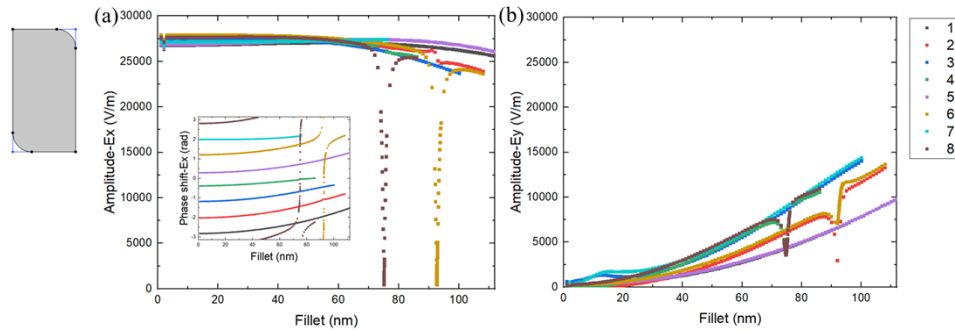


**Fig. 7.** The effect of the 2 diagonal fillets of rectangular pillars on the amplitudes and the phase shifts of the transmitted light for (a) x-polarization and (b) y-polarization.

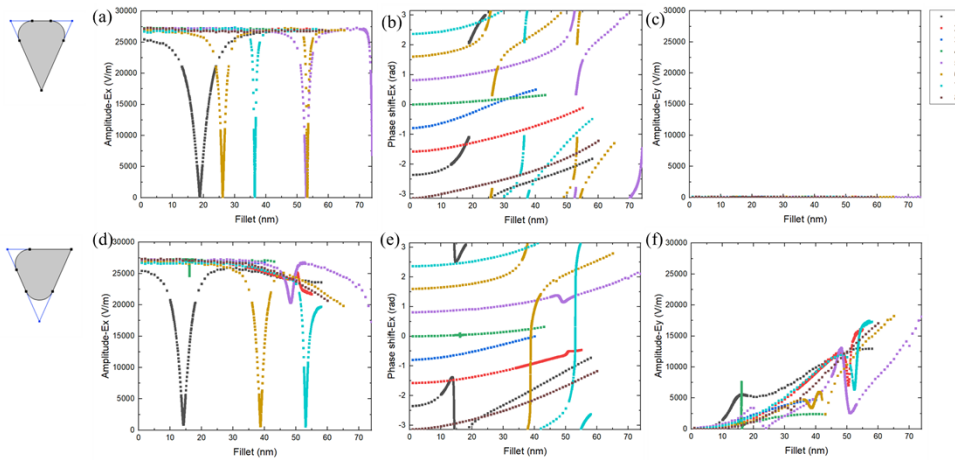


**Fig. 8.** The effect of the 2 symmetric fillets of isosceles triangular on the amplitudes of (a) x-polarization and (b) y-polarization, and the phase shifts of (c) x-polarization. The effect of the 2 asymmetric fillets of isosceles triangular on the amplitudes of (e) x-polarization and (d) y-polarization, and the phase shifts of (f) x-polarization.

shown in Fig. 6(d). The BICs from this structure exist only at certain wavelengths. The phase shift is very sensitive to the wavelength because the size of the structure is near to the wavelength.

In the other hand, in the case of 2 diagonal fillets of the rectangular pillars, where the symmetry is broken, the amplitude of the x-polarized transmitted light begins to reduce when the radius of the fillet is large enough (near the maximum), as shown in Fig. 7(a). Figure 7(b) shows that the energy is leaked to y-polarization from x-polarized light. The cases of 1 fillet and 3 fillets are shown in Fig. S2 and Fig. S3 (Supplement 1), respectively. The break of the original symmetry of the rectangular pillar results in the leakage from x-polarized light.

For isosceles triangular pillars, 2 asymmetric fillets break the original symmetry, while 1 fillet, 2 symmetric fillets and 3 fillets don't break the original symmetry. The effects of the 2 symmetric fillets to the amplitudes and phase shifts of the transmitted lights are shown in Fig. 8(a), (b) and (c). Similar to the case of rectangular pillars, the BICs and quasi-BICs also exist at certain specific fillet radii. The amplitude remains almost constant, and the phase shift increases gradually with the increase of fillet radius, excluding the BIC and quasi-BIC. Specially, the amplitude of the transmitted light can't remain constant when the radius of the fillet is large enough in Fig. 8(d) and (f), where the fillets are introduced to 2 asymmetric corners of

the isosceles triangular pillars. This is mainly due to the break in the axis of symmetry of the isosceles triangular pillar. Compared to the rectangular pillars, it is much easier to find the BICs in isosceles triangular pillars in our simulation. Additionally, even when the radius of the fillets is as small as about 10 nm, the quasi-BIC still exists, such as the pillar 1 (the black spots). This means that a small error of the geometric parameters for isosceles triangular pillars may induce a large amplitude and phase change of the transmitted light. The cases of 1 fillet and 3 fillets are shown in Fig. S4 and Fig. S5 (Supplement 1), respectively.

#### 4. Conclusion

In conclusion, we numerically study the dielectric metasurface with meta-atoms of rectangular and isosceles triangular pillars. We select 8 pillars for both rectangular pillars and isosceles triangular pillars to cover the entire  $2\pi$  phase shift of the transmitted light. While rectangular pillars can function as half-wave plate, isosceles triangular pillars cannot. The modulation of the isosceles triangular pillar to transmitted light is strongly related to the axis of symmetry of the pillar. We also introduce fillets to the corners of the rectangular pillars and isosceles triangular pillars under different symmetric conditions. For both types of pillars, we can find the bound state in continuum (BIC) while the radius of the fillets is changing. Apart from the BICs and quasi-BICs, the amplitudes of the transmitted light remain almost the same, and the phase shifts gradually increase with the increase of the radius of the fillets. However, for rectangular pillars, fillets introduced to 1 corner, 2 diagonal corners and 3 corners can cause the energy of x-polarization to leak to other states when the radius of the fillets is large enough. For triangular pillars, fillets introduced to 2 asymmetric corners can also reduce the energy of x-polarized light. Both of them are caused by the break in the original symmetry. These meta-atoms with fillets can find potential applications in the generation of accurate metasurface hologram, metasurface absorber, sensing and so on.

**Funding.** Amada Foundation (AF-2023201); Amano Institute of Technology.

**Acknowledgments.** We thank Dr. Liu and Dr. Li from the Tanaka Laboratory at Kyoto University for their assistance with the simulations for this work.

**Disclosures.** The authors declare no conflicts of interest.

**Data availability.** Data underlying the results presented in this paper are not publicly available at this time but may be obtained from the authors upon reasonable request.

**Supplemental document.** See Supplement 1 for supporting content.

#### References

1. N. Yu, P. Genevet, M. A. Kats, *et al.*, "Light propagation with phase discontinuities: generalized laws of reflection and refraction," *Science* **334**(6054), 333–337 (2011).
2. Y. Xie, W. Wang, H. Chen, *et al.*, "Wavefront modulation and subwavelength diffractive acoustics with an acoustic metasurface," *Nat. Commun.* **5**(1), 5553 (2014).
3. M. Jang, Y. Horie, A. Shibukawa, *et al.*, "Wavefront shaping with disorder-engineered metasurfaces," *Nat. Photonics* **12**(2), 84–90 (2018).
4. H. L. Zhu, S. W. Cheung, K. L. Chung, *et al.*, "Linear-to-circular polarization conversion using metasurface," *IEEE Trans. Antennas Propag.* **61**(9), 4615–4623 (2013).
5. Y. Yang, W. Wang, P. Moitra, *et al.*, "Dielectric meta-reflectarray for broadband linear polarization conversion and optical vortex generation," *Nano Lett.* **14**(3), 1394–1399 (2014).
6. J. P. Balthasar Mueller, N. A. Rubin, R. C. Devlin, *et al.*, "Metasurface polarization optics: independent phase control of arbitrary orthogonal states of polarization," *Phys. Rev. Lett.* **118**(11), 113901 (2017).
7. N. Lawrence, J. Trevino, and L. Dal Negro, "Aperiodic arrays of active nanopillars for radiation engineering," *J. Appl. Phys.* **111**(11), 113101 (2012).
8. L. Chen, Q. Ma, H. B. Jing, *et al.*, "Space-energy digital-coding metasurface based on an active amplifier," *Phys. Rev. Appl.* **11**(5), 054051 (2019).
9. X. Ni, A. V. Kildishev, and V. M. Shalaev, "Metasurface holograms for visible light," *Nat. Commun.* **4**(1), 2807 (2013).
10. G. Zheng, H. Muhlenbernd, M. Kenney, *et al.*, "Metasurface holograms reaching 80% efficiency," *Nat. Nanotechnol.* **10**(4), 308–312 (2015).

11. X. Guo, M. Pu, Y. Guo, *et al.*, “Flexible and tunable dielectric color meta-hologram,” *Plasmonics* **15**(1), 217–223 (2020).
12. A. W. Lohmann and D. P. Paris, “Binary Fraunhofer holograms, generated by computer,” *Appl. Opt.* **6**(10), 1739–1748 (1967).
13. Q. Jiang, G. Jin, and L. Cao, “When metasurface meets hologram: principle and advances,” *Adv. Opt. Photonics* **11**(3), 518–576 (2019).
14. Q. Jiang, L. Cao, H. Zhang, *et al.*, “Improve the quality of holographic image with complex-amplitude metasurface,” *Opt. Express* **27**(23), 33700–33708 (2019).
15. S. Zhang, M. H. Kim, F. Aieta, *et al.*, “High efficiency near diffraction-limited mid-infrared flat lenses based on metasurface reflectarrays,” *Opt. Express* **24**(16), 18024–18034 (2016).
16. M. Khorasaninejad, A. Ambrosio, P. Kanhaiya, *et al.*, “Broadband and chiral binary dielectric meta-holograms,” *Sci. Adv.* **2**(5), e1501258 (2016).
17. J. Kim, D. K. Oh, H. Kim, *et al.*, “Metasurface holography reaching the highest efficiency limit in the visible via one-step nanoparticle-embedded-resin printing,” *Laser Photon. Rev.* **16**(8), 2200098 (2022).
18. A. Arbabi, Y. Horie, M. Bagheri, *et al.*, “Dielectric metasurfaces for complete control of phase and polarization with subwavelength spatial resolution and high transmission,” *Nat. Nanotechnol.* **10**(11), 937–943 (2015).
19. J. Tian, Q. Li, P. A. Belov, *et al.*, “High-Q all-dielectric metasurface: super and suppressed optical absorption,” *ACS Photonics* **7**(6), 1436–1443 (2020).
20. A. Lochbaum, Y. Fedoryshyn, A. Dorodnyy, *et al.*, “On-chip Narrowband Thermal Emitter for Mid-IR Optical Gas Sensing,” *ACS Photonics* **4**(6), 1371–1380 (2017).
21. T. Inoue, M. De Zoysa, T. Asano, *et al.*, “Realization of Narrowband Thermal Emission with Optical Nanostructures,” *Optica* **2**(1), 27–35 (2015).
22. L. Carletti, K. Koshelev, C. D. Angelis, *et al.*, “Giant nonlinear response at the nanoscale driven by bound states in the continuum,” *Phys. Rev. Lett.* **121**(3), 033903 (2018).
23. J. Wang, P. Li, X. Zhao, *et al.*, “Optical bound states in the continuum in periodic structures: mechanisms, effects, and applications,” *Photonics Insights* **3**(1), R01 (2024).
24. F. Binkowski, F. Betz, R. Colom, *et al.*, “Poles and zeros in non-Hermitian systems: Application to photonics,” *Phys. Rev. B* **109**(4), 045414 (2024).